The Sackler Colloquium on promises and perils in nanotechnology for medicine

Robert H. Austin[a] and Shuang-fang Lim[b,1]

[a]Department of Physics, Princeton University, Princeton, NJ 08544; and [b]Department of Physics, North Carolina State University, Raleigh, NC 27695-7612

The Sackler Colloquium entitled ''Nanomaterials in Biology and Medicine: Promises and Perils'' was held on April 10–11, 2007. We have been able to assemble a representative sampling of 17 of the invited talks ranging over the topics presented. Any new technology carries with it both a promise of transforming the way we do things and the possibility that there are unforeseen consequences. The papers collected here represent a cross-section of these issues. As an example, we present our own work on nano-upconversion phosphors as an example of this new class of nanomaterials with potential use in medicine and biology.

nanomaterials | upconversion

Every so often, there exists a technology breakthrough that changes how we look at things, and how we do things. Often, in the first flush of exploration, things seem to be too good to be true, and this is often the case. Right now, we are in the latter stages of the beginning of the nanotechnology revolution. Billions of dollars are being poured into nanotechnology, and rather extreme claims are being made, on both the positive and the negative sides. It certainly is true that we have to be careful. Perhaps 2 quick stories can serve as a sobering reminder of nanotechnologies gone awry. The philosophy in organizing this Colloquium was to try to put a balanced perspective in the role of nanotechnology in biology and medicine; we wanted the speakers to not only present the very cutting edge of nanotechnology but also to remind us of the dangers of unchecked technological growth that ignores the complexity and sensitivity on long time scales of biological systems. The Colloquium was organized around 4 main themes: (*i*) new technologies to create functional nanomaterials, (*ii*) societal and ethical concerns of nanotechnology in medicine, (*iii*) functional nanomaterials in biology, and (*iv*) frontiers in nanotechnology. George Whitesides presented the 7th Annual Sackler Lecture on ''Nanotechnology: A Portrait in Early Adolescence.''

To understand the concerns expressed about nanotechnology, it is important to look at the history of materials that had a strong nano content before the term became fashionable. Asbestos was once a wonder material, renowned for its softness when woven into fabric yet its remarkable flame-retardant ability. It is a very complex mineral; the most common form of it [chrysotile, $Mg_3(Si_2O_5)(OH)_4$] is found world-wide and has been known since ancient times (1). The Romans used it as the perfect table cloth mate-

rial: after the meal was done, you could throw it into the fire and out it would come, sterile and clean. Yet even the ancient Romans and Greeks knew that asbestos seemed to affect the lungs of workers. Pliny the Elder advised prospective buyers of slaves to avoid young quarry workers; they seemed to die young. Yet, despite these warnings about the material that stretch back for thousands of years, during the 20th century, asbestos was used extensively for its unique insulating and fire-retardant properties, among many other things. In a tragic twist of irony, the first filtered cigarettes in the 1950s used asbestos as part of the filter (2). R.H.A.'s own house in Princeton was clad in asbestos when purchased 30 years ago. It was great to paint; the paint never peeled off because the asbestos was totally impermeable to water, and of course at least the skin of the house was basically fireproof. All of the floor tiles in Jadwin Hall, the building that houses Princeton University's Physics Department, are asbestos.

But asbestos can easily become a nanomaterial, and therein literally lies the rub. Asbestos has 3 cleavage planes, but 2 are very weak, so the material tends to form long fibrils. These fibrils are easily cleaved to ultimately form fibers, which can be as narrow as 10 nm. These extremely thin but long fibers, once airborne, lodge in the lungs, and because of the remarkable chemical stability of asbestos are not removed easily. As you can see from Fig. 1, the topology of the asbestos fibers is extremely complex and acts as an irritant to the lung. As the New Yorker Magazine amply documented (3), the story of the full realization of the dangerous properties of asbestos fibers, although it should have been clear from the historical record, was slow to develop in the 20th century and, tragically, actively fought by companies involved in asbestos man-

ufacture. The net result has been many thousands of lives lost and damaged, $70 billion in litigation, and a bonanza for lawyers (4). Asbestos is an accidental nanomaterial that turned into an unmitigated disaster, because the nanoscale size of the fibers resulted in sequestration in the lung, a subject we will return to.

Asbestos has several different crystallographic forms, but the main problem of asbestos lies in the nanoscale diameter and micrometer-scale length of the fibers but not any overt chemical property. However, nanomaterials are interesting, not only because the physical properties of materials can be different as one goes down in size but also because the chemical properties can change quite dramatically. An example is titanium dioxide, TiO_2. Titanium dioxide is another material that has been embraced by the modern world for its marvelous properties, one of the chief of which is the high optical index of refraction of one of the crystallographic forms of titanium dioxide, the rutile form. The rutile crystallographic form of titanium dioxide has an optical index of refraction of 2.7 and hence when ground into a fine powder strongly scatters light. Thus, one of the main uses

The authors declare no conflict of interest.

This article is a PNAS Direct Submission.

© 2008 by The National Academy of Sciences of the USA

Fig. 1. SEM picture of asbestos fibers (6).

for titanium dioxide is as a sunscreen agent and a white base for a huge number of paints and coloring agents; it accounts for 70% of the total production volume of pigments worldwide (5). The rutile form of titanium dioxide is relatively chemically inert and is in bulk the most stable form of titanium dioxide, but there are 2 other common metastable forms of titanium dioxide, the anaphase and brookite forms. Fig. 2 shows the unit cells of the rutile and anaphase forms of titanium dioxide.

The anaphase form is of great interest, because it has the same tetragonal symmetry as the rutile form but is chemically quite different: when excited by UV light, the anaphase crystallographic form of titanium dioxide is a photocatalyst that can hydrolyze water; the highly reactive radicals created by the combination of UV + anaphase titanium dioxide is known to damage DNA (http://usgsprobe.cr.usgs.gov/picts2.html; ref. 6). Of course, the combination of UV and water is exactly the environment where titanium dioxide is used in sunscreens, so one would want to make sure the titanium dioxide is in the rutile, not the anaphase, form! Unfortunately, although the rutile form is stable in bulk, as the particulates drop in size below ≈100 nm, the relative stability of the rutile vs. anaphase forms becomes a function of pH and solvent because of the increasing surface/volume ratio (7). It is quite possible to have a nanopar-

ticulate suspension of titanium dioxide, which is largely the highly reactive anaphase form.

There are now some rumblings in the literature that indeed nanocrystals of titanium dioxide might have adverse impacts on biological systems (5), especially if the nanoparticulates are not controlled for proper thermodynamic phase forms. The lesson here is that the promise of nanomaterials in medi-
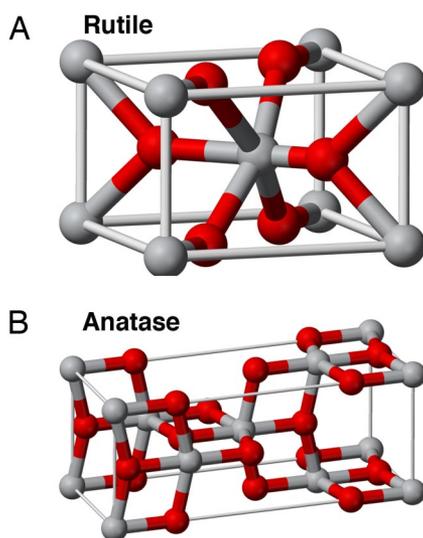

Fig. 2. Crystal structures of the 2 forms of titanium dioxide. (*A*) Thermodynamic stable bulk rutile unit cell of titanium dioxide. (*B*) Anaphase unit cell, which in nanocrystals and under certain solvent conditions can be the stable phase.

cine and biology has inevitably associated with it a peril that often is entirely not anticipated at the start, simply because we do not have a deep enough understanding of what happens as we go to the nanometer scale on many levels, and that lack of a deep understanding actually can have huge consequences to society.

Our Own Work in New Nanomaterials: Upconversion Phosphors (UCPs)

One of the authors of this paper, S.-f.L., presented her work on upconversion nanoparticles at the Sackler Conference, and we thought it would be informative to present part of that talk as an example of what is happening in new nanomaterials for biology and medicine. UCP are ceramic materials in which rare earth atoms (from the 15 elements with atomic numbers 57–71 comprising the lanthanide series) are embedded in a crystalline matrix. The rare earth ions have optical transitions arising from buried atomic 4f electronic orbitals, which typically absorb ≈970–1,000 nm in a series of lines of ≈2- to 5-nm width. Upconversion occurs via sequential excitation of a series of real, as opposed to virtual, levels as in conventional 2-photon dyes (8). The upconversion mechanism into the visible spectral region can occur as sequential excitation of the same atom or more typically excitation of 2 centers and subsequent energy transfer (9–11). The emission of UCPs consists of sharp lines characteristic of atomic transitions in a well-ordered matrix. Using different rare earth dopants, a large number of distinctive emission spectra can be obtained with colors from red to blue. Because the upconversion process occurs sequentially through real states, relatively low-power densities can be used for efficient upconversion, and UCPs have recently attracted substantial interest in both academia and industry for the purpose of labeling biological specimens (12, 13). Because the emitted light is upconverted to shorter wavelengths than the excitation wavelength, background fluorescence is virtually nonexistent.

The main advantages of UCP nanoparticle imaging for use in cells and tissue are the lack of autofluorescence by the specimen, absence of bleaching, multicolor imaging, and high-resolution cathodoluminescent imaging in a SEM (14). With the interest in imaging organisms at the subcellular level (15), nanoparticles in the sub-10-nm range are required, such as UCPs. Currently a great impediment to using UCPs in biological labeling applications is their size, a point that quantum dots and organic

Austin and Lim

dyes have excelled in. Solution-stable, unaggregated, bright upconverting, oxide-based phosphors have previously been demonstrated for submicron sizes. As one might expect from the titanium dioxide story we related, the crystal structure of these nanomaterials is quite important for how they function, but unfortunately in ways we do not understand. In the case of the UCPs, the crystal matrix is of importance, because it is believed that low phonon energy can reduce nonradiative loss due to the multiphonon relaxation and thus enhance the upconversion quantum efficiency (17, 18). The phonon spectrum of a matrix strongly depends on the crystallographic structure, and as we have seen for titanium dioxide, the thermodynamically stable phase is a function of particle size and is influenced by the solvent and the surface/volume ratio increases.

Thus, achieving a combination of the sub-10-nm particle size, low aggregation of the nanoparticles, size uniformity, high crystallinity required for high upconversion efficiency, and efficient surface functionalization has proven elusive to the present. However, we have been able to synthesize sub-10-nm, low-aggregating, upconverting nanophosphors that can be suspended in a solvent at very low aggregation levels. We synthesized the sub-10-nm rare earth-doped yttrium oxide-based nanophosphors by a flame spray pyrolysis process, using a liquid precursor. To facilitate complete and even combustion at sufficient flame temperatures, we chose a precursor consisting of ethanol as a fuel and yttrium and rare-earth complexes with 2-ethylhexanoic acid (2-EHA) as a source of the host and dopants, respectively. The reaction itself proceeded in a custom-built 10-cm-long alumina Laval tube (19). The Laval tube was chosen because it achieves an ultrashort exposure of the synthesized particles to high temperatures and thus suppress Ostwald ripening and particle aggregation. In our process, the organic precursor aerosol is ignited in the apex of a Laval tube, and combustion takes place in the exit cone. The temperature of the pyrolysis as measured by a type K thermocouple was ≈1,200°C at a distance of 1 inch downstream from the apex of the Laval tube. In the process, the precursor is first atomized in O_2 using a nebulizer (Micromist, Glass Expansion). The jet is then directed at the entrance of a Laval tube made of alumina. A methane torch provides the ignition for the flame, and the reactor temperature is controlled with a resistive wire heater. Phosphors were collected on a stainless steel cylinder kept at ≈100° C.
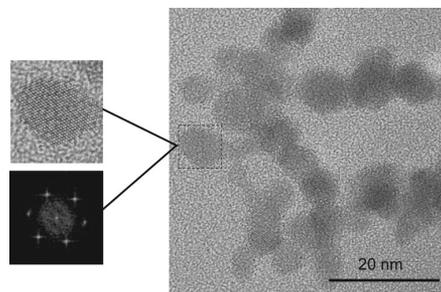
Fig. 3. HRTEM image of upconverting nanophosphor from the 2-EHA based precursor, showing selected nanoparticle and its corresponding Fourier transform diffraction pattern. The nanophosphor size and distribution were analyzed by a Philips CM200 FEG-TEM. Nanophosphors for electron microscopy were collected during spray pyrolysis directly onto TEM Cu-grids coated with holey carbon film.

Fig. 3 shows a high-resolution transmission electron microscopy (HRTEM) of the nanoparticles and the Fourier transform diffraction pattern. In the HRTEM image, facetted spheroidal nanoparticles with well-defined lattice structures are seen. The measured lattice spacing of the selected nanocrystal is 3.16 Å, consistent with the known lattice spacing of the (222) plane of cubic Y_2O_3 (Powder Diffr File JCPDS 65-3178, International Center for Diffraction Data). That orientation also appears to be the most frequently observed lattice orientation among the other nanocrystals shown. The corresponding particle size distribution, calculated from >220 nanoparticles, is shown in Fig. 4A. The distribution appears to demonstrate highly uniformly sized nanocrystals, with a mean size of 6.3 ± 1.3 nm.

The X-ray diffraction (XRD) spectrum in Fig. 5 shows several diffraction peaks that can be indexed to the standard Y_2O_3 body-centered cubic (bcc) phase. The bcc phase combined with the spheroidal shape of the nanophosphors obtained is a result of the high-synthesis temperature of our flame spray pyrolysis system. The nanoparticle size as calculated from Scherrer's equation (20) was ≈9 nm. The Y_2O_3 lattice constant, obtained by calculations using XRD data of the nanocrystals, is 10.5 Å, which is consistent with that of bulk Y_2O_3. The disparity of the sizes as measured by TEM and XRD can be attributed to the difference in quality of the nanophosphors, which is due to the different sample collection times during flame spray pyrolysis. For TEM analysis, only a small quantity of nanophosphors was collected directly onto TEM grids for ≈15 sec. In contrast, for XRD analysis, a much larger quantity of nanophos-
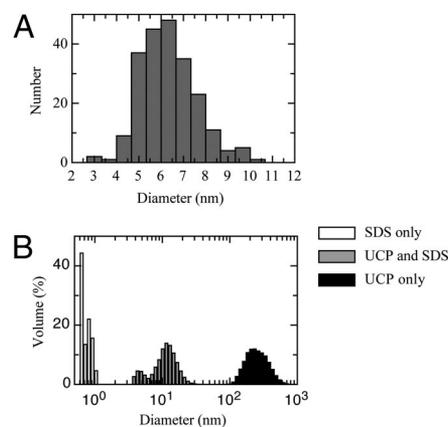
Fig. 4. Analysis of nanoparticle sizes. (*A*) Particle size distribution of nanophosphors obtained from the 2-EHA based precursor. (*B*) Volume distribution of sub-10-nm nanophosphors suspended in THF, with and without SDS. Particle size distributions in suspension were measured by using dynamic light scattering on a Malvern Zetasizer Nano-ZS (Malvern Instruments).

phors was required, which had to be collected over several hours during spray pyrolysis. Over the long time period, a slight change in spray conditions may have produced variations in size uniformity. This results in a larger size estimated by XRD analysis. However, as shown by TEM data, maintaining size uniformity is possible if spray conditions are strictly controlled. This can be achieved, for example, by installing mass flow controllers to ensure constant flame temperature and aerosol droplet size. Elemental analysis was performed on the flame spray-pyrolyzed upconverting nanophosphors by energy-dispersive X-ray spectrometry (EDX) on a Princeton Gamma Tech Integrated Dispersive X-Ray Microanalyzer (Princeton Gamma Tech, Princeton). The sub-10-nm phosphor showed preferential doping of the rare earth Yb over the rare earth Er (8.4 atomic percentage) doping over Er (6.8 atomic percentage) doping.

As it is our aim to use these nanophosphors for biological imaging; the ability to suspend these particles in aqueous media stably is crucial. Hence,

Fig. 5. The XRD spectrum showing sub-10- (broken line) and 40-nm particles (solid line).

an understanding of the behavior of the material in water is required. The isoelectric point (IEP) of yttrium oxide ranges from 8.6 to 9.1 (21). Below this pH range, there is a strong possibility of dissolution of yttrium oxide. The rate of dissolution will be further accelerated by the larger surface area of nano-sized yttrium oxide. At a pH above the IEP, we expect dissolution to be still significant for ultrasmall particles. In most biological applications, the pH used is usually below the pH range tolerated by yttrium oxide. Therefore, these nanophosphors have to be surface-modified to confer robustness over a large pH range. To that end, we have a silanized PEG coating on our nanophosphors when used with buffer solutions. However, this step is not necessary if the nanophosphors are suspended in non-aqeous solvents. For silanization of the 10-nm nanophosphors, 1 mg of the nanophosphors was dispersed in 1 mL of deionized water by probe-tip sonication at 10–12 W (root-mean-square) output power for ≈5 sec (Model 100, Fisher Scientific Sonic Dismembrator). To the suspension, an additional 2.3 mL of deionized water was added, followed by 30 mL of methanol and 200 μL of methoxy(polyethyleneoxy)propyl-trimethoxysilane (PEG-silane) (SIM6492.7, Gelest). The suspension was stirred for 2 h, heated to 60°C for 5 min, and then cooled. The nanophosphors were washed with centrifugation, twice with methanol, twice with methanol:deionized water (1:1), and twice with deionized water, and finally concentrated using centrifugal filter devices (Amicon Ultra-15, molecular weight cutoff 100,000). The resulting PEG-coated nanophosphors in water were transparent to the eye and displayed luminescence when excited with 980-nm illumination.

We have characterized in solution the PEG-silanized nanophosphors by using a combination of light scattering and zetapotential measurements. We have measured 50- to 60-nm diameter-sized PEG-silanized nanophosphors in water (Fig. 6), with a zetapotential of +17 mV at pH 5 and −37 mV at pH 9. With light scattering measurements, the hydrodynamic radius measured in solution is larger than that measured by the TEM in powder form, because of the balance of van der Waals forces, viscous flow, and Brownian motion in solution.

Of course, synthesis of nanoparticulates is one thing, but what they do in living tissue is quite another issue and, as we discussed in the sad story of asbestos, it can be quite surprising and discouraging to find that a nanomaterial can be quite toxic to living systems de-

Fig. 6. Volume distribution of PEG-silanized nanophosphors suspended in ultrapure water showing pH dependence. Particle size distributions in suspension were measured by using dynamic light scattering on a Malvern Zetasizer Nano-ZS (Malvern Instruments).

spite the wonderful properties. At this point, we have done only simple tests as to the influence of these nano-UCPs in tissue, in our case, nematides. The viability of the PEG-coated nanophosphors was tested in the digestive system of the nematode worm *C. elegans*. A similar protocol used in our previous studies (11) was followed for inoculation of the worms and transferring onto slides and for imaging using 2-photon microscopy. The dependence of the luminescence intensity was determined by integrating the emission from 1 particle in the field of view and varying the illumination intensity. Upconversion luminescence spectra were collected by using a fiber-coupled CCD spectrometer (Ocean Optics). Fig. 7A shows the visible emission from the PEG-coated sub-10-nm nanophosphors in the digestive system of the *C. elegans* worm under infrared illumination. The worms were monitored continuously for up to 24 h without any apparent change in the phosphors, as in blinking or bleaching, and in the condition of the worms. Because the worms were deprived of food, excretion also ceased, and the nanophosphors were still retained in them. Of course, if we are to use these UCPs as agents in applications ranging from tissue visualization to chemotherapy technologies will have to be developed for the specific labeling of the nanoparticle surface with tissue-specific probes.

Conclusions

This special section of PNAS will present a broad spectrum of papers that address the promise and perils of nanotechnology in medicine. We gave a brief historical overview of 2 cautionary tales, 1 still ongoing, of how nanotechnology has had unforeseen consequences in biology, and used our own work in UPCs to give an example of how nanotechnology is still is the adolescent stages of growth. The lessons of asbestos have been learned, and despite the great rush into nanomaterials, there certainly is a

Fig. 7. Images of nanoparticles with *C. elegans*. (*A*) False-color 2-photon images of *C. elegans* at 980-nm excitation with green representing the bright field and red for the PEG-silanized sub-10-nm nanophosphor emission at 60× magnification. (*B*) Combined image of 40-nm nanophosphor-fed worm with gray representing the SEM image, and red representing the cathode luminescence (CL) image. The CL image was obtained by monitoring the total light intensity from the sample by using a photomultiplier tube, without any color filtering. The sample was tilted at a 45° angle to the incoming beam, leading to some topography-induced contrast in the CL image.

heightened awareness of the potential problems that exist. For example, although Nanomedicine Summit 2008 presents a huge number of potential applications of nanotechnology to medicine (www.nanomedicinesummit.org/agenda.asp), we also note there are serious concerns to be addressed (22). We hope this paper acts as an introduction to the papers that follow, and that the reader will be made aware of all the issues that still need to be addressed as this new technology matures.

1. Alleman JE, Mossman BT (1997) Asbestos revisited. *Sci Am* 277:70–75.
2. Longo WE, Rigler MW, Slade J (1995) Crocidolite asbestos fibers in smoke from original Kent cigarettes. *Cancer Res* 55:2232–2235.
3. Brodeur P (1985) The New Yorker, July 1, p 3.
4. Surowiecki J (March 6, 2006) Asbestos, Inc. *The New Yorker*, p 33.
5. Winkler J (2004) *Titanium Dioxide* (Elsvier, Amsterdam).
6. Dunford R, *et al.* (1997) Chemical oxidation and DNA damage catalysed by inorganic sunscreen ingredients. *FEBS Lett* 418:87–90.
7. Finnegan MP, Zhang HZ, Banfield JF (2007) Phase stability and transformation in titania nanoparticles in aqueous solutions dominated by surface energy. *J Phys Chem C* 111:1962–1968.
8. Webb WW (2006) Commentary on the pleasures of solving impossible problems of experimental physiology. *Annu Rev Physiol* 68:1–28.
9. Auzel F (2004) Upconversion and anti-Stokes processes with f and d ions in solids. *Chem Rev* 104:139–173.
10. Corstjens PLAM, *et al.* (2005) Infrared up-converting phosphors for bioassays. *IEE Proc* 152:64–72.
11. Kuningas K, Rantanen T, Ukonaho T, Lovgren T, Soukka T (2005) Homogeneous assay technology based on up-converting phosphors. *Anal Chem* 77:7348–7355.
12. van de Rijke F, *et al.* (2001) Up-converting phosphor reporters for nucleic acid microarrays. *Nat Biotechnol* 19:273–276.
13. Corstjens PLAM, *et al.* (2008) Up-converting phosphor technology-based lateral flow assay for detection of Schistosoma circulating anodic antigen in serum. *J Clin Microbiol* 46:171–176.
14. Lim SF, *et al.* (2006) In vivo and scanning electron microscopy imaging of upconverting nanophosphors in *Caenorhabditis elegans*. *Nano Lett* 6:169–174.
15. Xie XS, Choi PJ, Li GW, Lee NK, Lia G (2008) Single-molecule approach to molecular biology in living bacterial cells. *Annu Rev Biophys* 37:417–444.
16. Kumar Challa SSR, ed (2006) *Nanomaterials—Toxicity, Health and Environmental Issues* (Wiley, Amsterdam).
17. Zhang JJ, *et al.* (2005) Mechanisms and concentrations dependence of up-conversion luminescence in Tm3+/Yb3+ codoped oxyfluoride glass-ceramics. *Phys Lett A* 337:480–486.
18. Kishimoto S, Hirao K (1996) Intense ultraviolet and blue upconversion fluorescence in Tm3+-doped fluoroindate glasses. *J Appl Physiol* 80:1965–1969.
19. Kim YJ, Wyslouzil BE, Wilemski G, Wolk J, Strey R (2004) Isothermal nucleation rates in supersonic nozzles and the properties of small water clusters. *J Phys Chem A* 108:4365–4377.
20. Schlenker JL, Peterson BK (1996) Computed X-ray powder diffraction patterns for ultrasmall zeolite crystals. *J Appl Crystallogr* 29:178–185.
21. Yasrebi M, ZiomekMoroz M, Kemp W, Sturgis DH (1996) Role of particle dissolution in the stability of binary yttria-silica colloidal suspensions. *J Am Ceram Soc* 79:1223–1227.
22. Maynard AD, *et al.* (2006) Safe handling of nanotechnology. *Nature* 444:267–269.

Austin and Lim